

# Sparse Representation-based Classification of Geomagnetically Induced Currents

Mohammad Babakmehr<sup>\*</sup>, *IEEE Member*, Farnaz Harirchi<sup>†</sup>, *IEEE Member*, Moazzam Nazir<sup>‡</sup>, *IEEE Student Member*, Shiyuan Wang<sup>‡</sup>, *IEEE Student Member*, Payman Dehghanian<sup>‡</sup>, *IEEE Member*, Johan Enslin<sup>†</sup>, *IEEE Fellow Member*

<sup>\*</sup>*Global Data, Insights, and Analytics, Ford Motor Co, Dearborn, Michigan*

<sup>†</sup>*ECE Department, Clemson University Restoration Institute, Charleston, South Carolina*

<sup>‡</sup>*ECE Department, George Washington University, Washington, D.C.*

**Abstract**—Geomagnetically Induced Currents (GIC) are the significant effects of the Geomagnetic Disturbances (GMDs) on power systems. GICs typically appear in the form of DC components in the current waveforms of high voltage transmission lines and may lead to transformer saturation, so-called DC saturation. Such saturation scenarios, if experienced, can result in severe damages to the transformer core and significantly increase the system-wide risk of major blackouts. It calls for developing detection and classification mechanisms for GICs in power systems so they can be prevented or interrupted before emerging as a threat. A major challenge associated with GIC detection is the presence of similar events, resulted from faults and other distortions, such as AC saturation caused by harmonics. The current signals recorded by current transformers can be analyzed to classify these events. In this paper, the time-frequency S-Transform is integrated with a sparsely-enhanced version of the collaborative representation-based classification to implement a fast, reliable, and adaptive GIC events classification approach. Unlike usual techniques, the proposed mechanism does not need any training procedure while, due to its linear formulation, acts inherently fast and is adaptable to recognize the challenging scenarios of combined events.

**Index Terms**— Smart grids, geomagnetically induced currents, transformer saturation, pattern recognition, sparse classification.

## I. INTRODUCTION

GEOMAGNETICALLY induced currents (GICs) have long been the cause of various power system failures, thus threatening the power system stability and security [1]. Although mitigation was traditionally the focus of research in GIC studies, the recent developments in sensing technologies bring about new opportunities to the table. Using real-time measurements from electrical currents, one can develop advanced analytical tools to detect and classify GICs from similar power quality events towards a successful and resilient GIC mitigation strategy. However, research and development efforts have not yet been focused on addressing such challenges.

### A. Overview and Literature Review

Nowadays, the combination of advanced signal processing and state of the art in artificial intelligence forms the main body of the most popular frameworks in event detection and classification in a variety of monitoring and control problems including those for power system [2]. Power system events classification can be interpreted in terms of a general pattern recognition (PR) problem, that is usually split into a standard 5-step procedure as follows [3]: (1) Measurement and preprocessing, (2) Potential event pattern detection from raw data, (3) Feature Extraction (FE) from the

pattern, that is widely approached by exploiting the Time-Frequency analysis including but not limited to Short Time Fourier Transform (STFT), Wavelets, S-transform, Time-Time Transform, Mathematical Morphology, etc. (please refer to [2]-[4] and references therein). (4) Feature Selection (FS) that is a set of techniques for dimensionality reduction within the feature space, thereby reducing the computational cost, and finally (5) Classification where each detected pattern is assigned to a certain class of events based on the available domain knowledge. Various methods are developed to study and implement each of these steps, including simple linear to highly complex and nonlinear algorithms, where the best approach should be selected by studying the data characteristics [5], [15].

Recently, signal analytics have been utilized in GIC-related studies. Authors of [6] developed a set of analytics to monitor GICs through processing the distorted electrical signals. These approaches, however, are not resilient to grid harmonics and their confusions with those of GICs. Studies in [8] revealed that as the GICs intensity changes, the harmonic current magnitudes of different orders change accordingly. The application of wavelet transforms (WT) for transformer overload detection has been investigated in [7].

Most recently, and inspired by the principle concepts of pattern recognition, the authors in [22] proposed a GIC detection mechanism in transmission networks. Well-recognized time-frequency analytics, i.e., the WT and STFT, were applied for FE while a deep learning neural network (DNN) was implemented for the sake of classification. On the one hand, a major challenge with the DNN classifier training remains to be the choice of the optimal number of training data samples while decreasing the computational complexity of the training process. On the other, due to the fixed window width limitations, STFT is not capable of accurately capturing the dynamics for non-stationary signals. WT, however, performs acceptably to extract the signal information in both time and frequency domains, while is known to be more sensitive to noise.

### B. Challenges, Motivations, and Contributions

For the sake of GIC detection and classification, two major sets of unresolved challenges exist among the implementation of the state-of-the-art PR-based algorithms: (1) Analytical modes, which are mostly associated with general algorithmic issues such as (1.1) optimal feature extraction, (1.2) Feature selection is used to reduce the dimensionality of feature space and further improve the computational efficiency, (1.3) Optimal classifier training. (2) Practical modes including (2.1) Computational resource

limitations in GIC observational points such as PMU measurements in primary and secondary sides of transformers or power inverters, (2.2) no consideration to the integrated information revealed from the 3-phase systems, (2.3) Scalability and vulnerability to noise and uncertainty sources.

In this paper, we address the FE shortages through an enhanced version of a time-frequency transform named S Transform proposed in [9]. The S transform is the variable-window version of the STFT or an extension of WT, principled based on a scalable localizing Gaussian window, supplies the frequency-dependent resolution, and entirely captures the local phase information. Moreover, the theory of sparse-based classification [19] is harnessed to formulate the GIC event Classification problem as a Sparse Recovery problem with lower time and implementation complexities (GIC-SRC).

The proposed SRC framework, has variety of advantages compared to the ordinary classifiers. It is training-free approach while it offers feature independency along with the fact of blless of dimensionality discussed in Section IV. Consequently, we do not need to put much efforts on conventional FE-FS and the parameter adjustments included in ordinary classifiers training steps. Different from the conventional classifiers, the collaborative formulation of the GIC-SRC results in higher sparsity in the proposed framework when the number of event classes increases, thereby revealing a better performance and noise robustness. These advantages, along with the linearity of the proposed GIC-SRC, considerably decrease our computational complexity and time cost while preserving a higher accuracy compared to the state-of-the-art classifiers. The performance of this method is verified over a comprehensive set of 12 GIC-polluted signal patterns. We will show the superiority of the proposed GIC-SRC algorithm in comparison with other trending algorithms such as ANN [16], and SVM, and its adaptability and scalability for unexpected or drastic changes in the data characteristics.

## II. PROBLEM DESCRIPTION AND TERMINOLOGY

Here we consider a balanced 110V-60Hz power system as our case study. A set of measurements including  $N = \sum_{j=1}^J n_j$  labeled 3- $\varphi$  sinusoidal electrical current signals are recorded from  $J$  classes of events and are available as the training dataset. Each of these known-class vectors,  $\mathbf{y}_i \in \mathbb{R}^M, i = 1, 2, \dots, N$  represents a possible disturbance event, presumably GIC-related events. The goal is to propose an algorithm that takes a feature vector,  $\mathbf{f}^{test}$  extracted from a sample of such events,  $\mathbf{y}^{test}$ , and assign it to one of the GIC-caused disturbance classes labeled as  $c_j, j = 1, 2, \dots, J$ . This integrated mapping is represented as a mathematical function  $c_i = A(D(\mathbf{y}^{test}))$ ,  $c_i \in \mathcal{C} = \{c_j | j = 1, 2, \dots, J\}$ , in which  $D$  stands for the feature extraction operator, while the classification is represented by the operator  $A$  (which is found through the classifier training and is a nonlinear map in general). The optimal framework for the selection of these mappings is a major topic in pattern recognition literature.

The proposed GIC-SRC first implements an enhanced time-frequency decomposition technique that harnesses the flexibilities of the S-transform in time-frequency plane tiling [12] for feature extraction (hence, the first operator  $D$  is implemented). A modified sparse representation-based classification methodology is next applied for the operator  $A$ . It features a reduced size of the feature vectors in the mapping  $D$ . An optimal training set selection approach is pursued to identify the most informative feature

vectors for each class of the disturbance event. We here split our proposed approach into two main sections: (i) Instantaneous 3-phase feature extraction via HS-Transform, (ii) Feature selection and classification using the informative sparse classifier. The entire procedure is termed here as Time-frequency-based Informative Sparse Classification for Geomagnetically Induced Currents (TISC-GIC), as demonstrated in Fig.1.

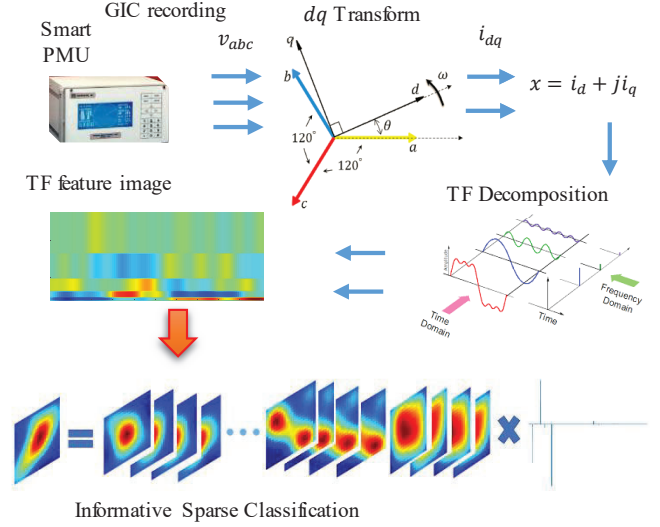


Fig.1. Time-frequency decomposition based Informative Sparse Classification for Geomagnetically Induced Currents (TISC-GIC)

## III. INSTANTANEOUS 3-PHASE FEATURE EXTRACTION

In this work, a simultaneous 3-Phase Time-Frequency feature extraction is presented primarily for GIC classification. Our approach consists of 3 major steps: (1) define an alternative complex representation of 3-phase signals using power theories, (2) use Hyperbolic S-transform to integrate the benefits of the STFT and multiscale resolution of Wavelets, (3) generate an enhanced HS-Scalogram distribution as feature-images.

### A. Instantaneous 3-Phase Signal Processing Tools: Direct-quadrature transformation ( $dq$ )

One may alternatively interpret a time-domain instantaneous power theory in terms of a 3D mathematical signal decomposition that maps a 3-phase waveform into a coupled, (if applicable) orthogonal feature space at each sample of time [10]. Every decomposed component in the newly formed feature space is referred to as an instantaneous power element [24]. We here employ a technique widely known as the Synchronous reference frame ( $dq$ ). It is a combination of Park, and Concordia transforms, which converts 3-phase electrical signals into a 2 dimensional but orthogonal space. Monitoring the trajectories of the Time-Frequency Representation (TFR) of 3-phase signals under this alternative mathematical representation can form a unique, fast, and real-time GIC identifier. The  $dq$  or Park-Clark transform from  $abc$  frame to the synchronous reference frame is defined as follows [10]:

$$\begin{bmatrix} i_d \\ i_q \end{bmatrix} = \sqrt{\frac{2}{3}} \begin{bmatrix} \cos(\theta) & \cos(\theta - \frac{2\pi}{3}) & \cos(\theta + \frac{2\pi}{3}) \\ -\sin(\theta) & -\sin(\theta - \frac{2\pi}{3}) & -\sin(\theta + \frac{2\pi}{3}) \end{bmatrix} \begin{bmatrix} i_a \\ i_b \\ i_c \end{bmatrix}. \quad (1)$$

Where  $\theta$  is the time-variant synchronization angle that represents the angular position of the  $dq$  frames. Consider the orthogonality between  $d$  and  $q$  components one may define a combined complex signal as follows:

$$x = i_d + j i_q \quad (2)$$

Although the general format of  $dq$  transforms has an extra power component, namely zero component that carries the unbalanced portion of the signal, for a balanced system,  $x$  carries the whole 3-phase information in this new 2-dimensional mathematical domain. We may now use the TFR of this complex signal  $x$  (for any GIC event captured on a 3-phase current) to form a distinctive feature space for GIC classification.

### B. Feature Extraction Through Hyperbolic S-Transform

During the last couple of decades, the Time-Frequency Representation has been a cutting-edge research area in studying the behavior of dynamic signals such as faults in electric power grids. Different from the Fourier transform, it offers simultaneous time-frequency information on the specifications of the signals' energy and power components [11].

The S-Transform (ST) is an alternative linear TFR developed first time by Stockwell et al. in [9], [12]. S-Transform integrates the local frequency analysis of the STFT with multiscale features of WT. It can be, therefore, characterized as a multiscale local FT. The STFT can capture transient frequency variations over time through a windowing operation that offers time localization. The choice of the window function is, however, challenging and involves a trade-off. Improving STFT, the progressive resolution in WT can be applied. However, it is worth noting that WT measures a similar quantity to a frequency called scale. The scale is not a characteristic feature of either phase information or measurements. FT, STFT, and WT are defined as follows:

$$\text{FT:} \quad X(f) = \int x(t') e^{-i2\pi f t'} dt' \quad (3)$$

$$\text{STFT:} \quad X_g(t, f) = \int x(t') g^*(t' - t) e^{-i2\pi f t'} dt' \quad (4)$$

$$\text{CWT:} \quad X_\psi(t, a) = \int x(t') \sqrt{a} \psi^*(a(t' - t)) dt' \quad (5)$$

where  $g$  is a window (e.g., Gaussian),  $\psi$  is a zero-mean mother wavelet function, and  $a = \frac{f}{f_0}$  is its associated scaling factor. The ST combined the globally referenced phase and frequency measurements from DFT and STFT, with the progressive resolution of the WT through the following formulation:

$$\text{ST:} \quad X(t, f) = \int x(t') \frac{|f|}{\sqrt{2\pi}} e^{-\frac{(t'-t)^2 f^2}{2}} e^{-i2\pi f t'} dt' \quad (6)$$

Compared to STFT, the constant width of the localizing time window is  $\frac{1}{|f|}$  in the ST. Hence, a choice of narrower time windows at higher frequencies and wider ones at lower frequencies is made, while the scale interpretation is replaced with the pure frequency.

Like its linear TFR ancestors, the ST suffers from a low TF resolution as well as the high computational complexity. In response, a variant fast discrete version of the ST is introduced in [14]. In order to address the localization disturbance challenges in

the time domain associated with the Gaussian window in (7), a Hyperbolic ST (HST) is employed [17], offering a way better time and frequency resolutions at low and high frequencies. We define the discrete version of the HST as follows:

$$\text{HST}(n, k) = \sum_{m=1}^N X(m, n) G(m, n) e^{-j \frac{2\pi}{N+1} m k} \quad (7)$$

where  $X(m, n)$  is the frequency-shifted discrete FT (DFT) of the discrete signal  $x(n)$ :  $X(m) = \frac{1}{N} \sum_{n=1}^N x(n) e^{-j \frac{2\pi}{N+1} m n}$ , and  $G(m, n)$  is the DFT of a hyperbolic window ( $h_w$ ) defined below:

$$h_w(t) = \frac{2f_s}{\sqrt{2\pi(\alpha+\beta)}} e^{-\frac{f_s^2 \varphi(t)^2}{2}} \quad (8)$$

$$G(m, n) = \frac{2f_s}{\sqrt{2\pi(\alpha+\beta)}} e^{-\frac{f_s^2 \phi(f)^2}{2}} \quad (9)$$

where  $\varphi(t)$  and  $\phi(f)$  are the general representations of a hyperbolic function as follows:  $\frac{\alpha+\beta}{2\alpha\beta} ((\tau - t - \xi) + \sqrt{(\tau - t - \xi)^2 + \gamma^2})$ . Additional details on the selection of the parameters  $\alpha, \beta, \gamma$ , and  $\xi$  are available in [18]. In order to maintain the quadratic dependence of the signal to assure the best possible time-frequency resolution, we take the squared amplitude modulus of the HST, termed as HS-Scalogram (HSCA= $|\text{HST}|^2$ ), as a feature-image that can be used for further classification purposes.

Figure 2.a-f represents a selected number of GIC-polluted 3-phase signals in addition to their HSCA feature-images. Although time invisible, the TFR using HS-transform can extract meaningful patterns of dissimilarity between these events that can be further used in the final classification step. All signals are generated in MATLAB/Simulink using the IEEE 34-bus test system. Of note is that these time-frequency images (Fig.2 a-f: bottom panels) are not a mathematical representation of the original 3-phase sinusoidal current signals but the associated complex-valued  $dq$ -transform representation as defined in (2). As such, one should not expect to find any dominant frequency component around 60 Hz within the frequency range.

## IV. INFORMATIVE SPARSE CLASSIFICATION

In this Section, an overview of the informative sparse GIC events classification approach is presented based on the sparse representation-based classification technique [19]-[20]. We briefly review the sparse recovery theorem concepts utilized to interpret and solve the GIC-event (GICE) classification problem.

### A. Sparse Representation-based GIC Events Classification

Consider  $N$  number of 3-phase GICE patterns from  $J$  GICE classes are recorded and available in 3-D vectors  $y_i$ . Using  $dq$ -transform an orthogonal complex alternative signal named  $x_i$  is generated (2). Next, the HS-Scalogram (7) of the signal  $x_i$  is computed and stored as a feature-image called  $f_i$ . We form, namely, a training feature tensor  $F = [f_1, f_2, \dots, f_N] \in \mathbb{R}^{(T \times M) \times N}$ , for the samples to from different classes, i.e.,

$$F = [F_1 | F_2 | \dots | F_J]. \quad (10)$$

where  $T$  and  $M$  indicate the number of pixels along the time and frequency axes, respectively.  $F_j$  indicates the feature sub-tensor formed by the concatenation of all feature images of training GICE samples associated with the  $j^{\text{th}}$  event class. According to the

sparse recovery theorems, if training data samples are fairly informative concerning the general behavior of the  $j^{th}$  class, any arbitrary new feature image  $f^{test}$  from a similar class can be approximately linearly-spanned by the corresponding training data; that is, for some real-valued vector  $s_j \in \mathbb{R}^{n_j}$ :

$$f^{test} = F_j s_j. \quad (11)$$

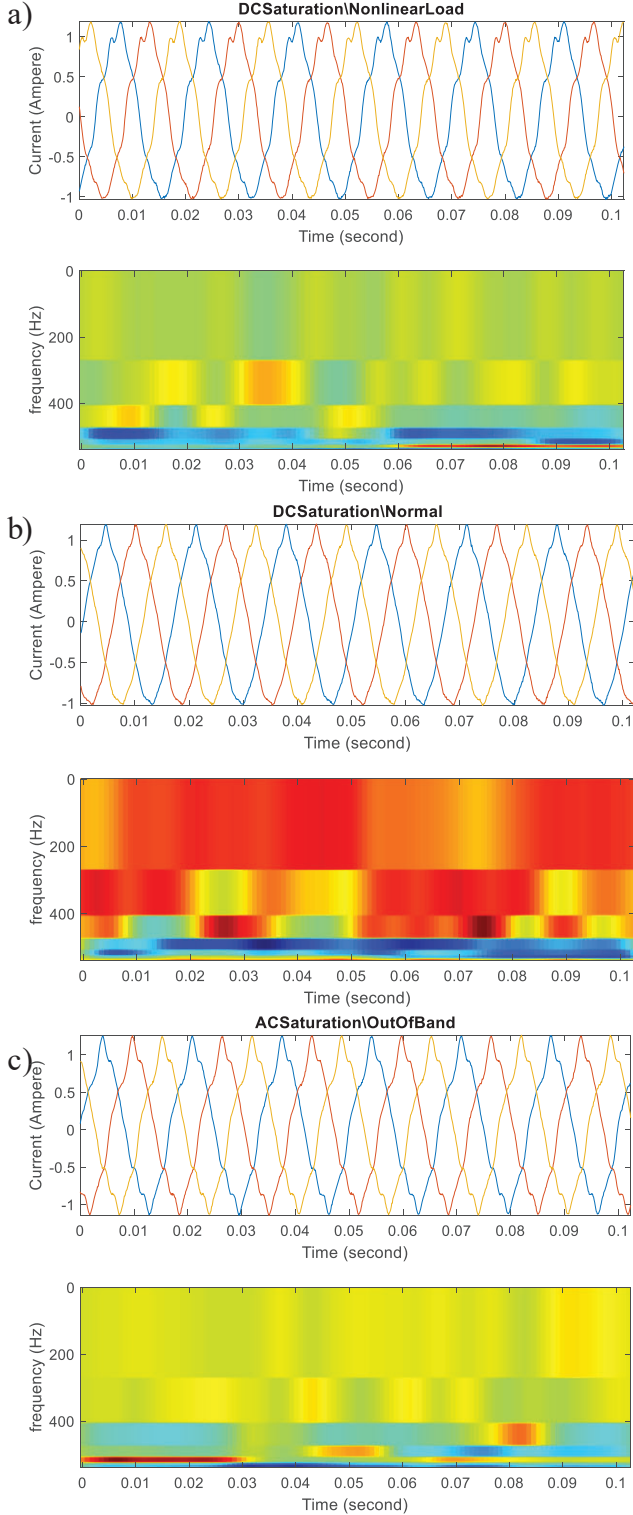


Fig 2.a-c are illustrating the time domain behavior of different GIC-related events on top in addition to their HS-T transform scalograms on the bottom

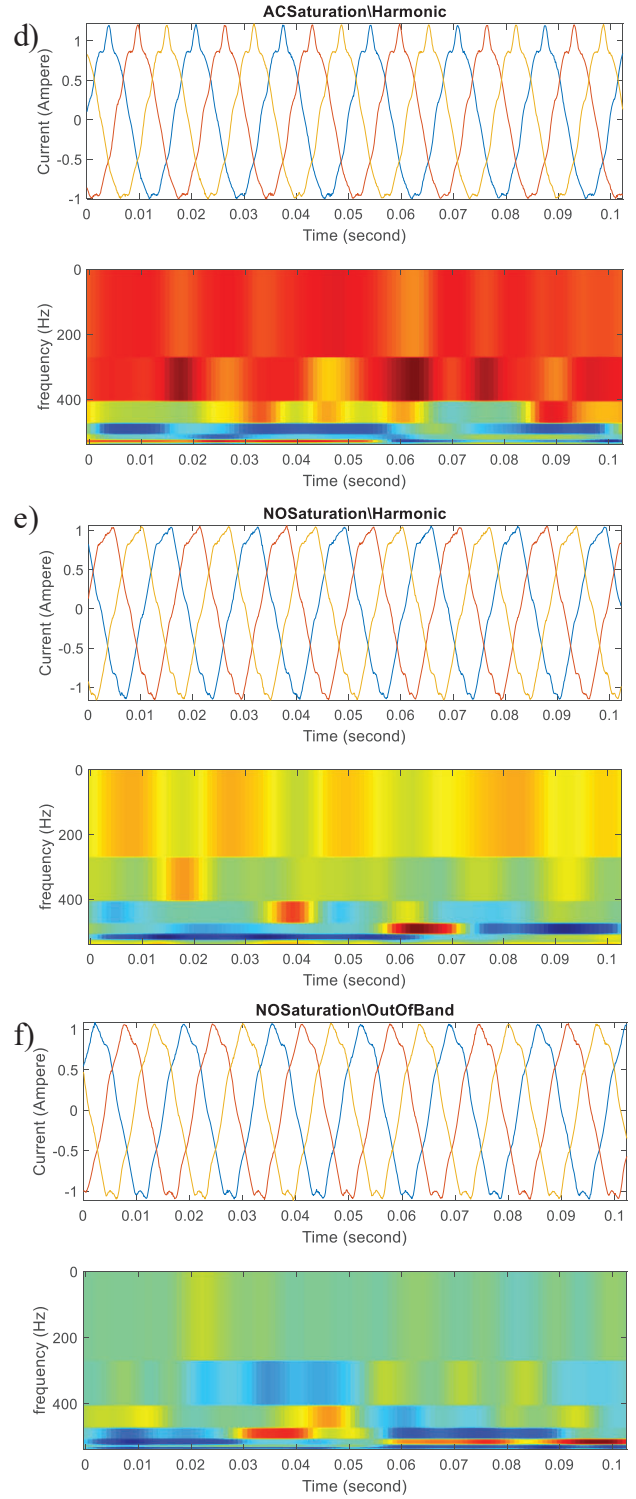


Fig 2.d-f are illustrating the time domain behavior of different GIC-related events on top in addition to their HS-T transform scalograms on the bottom

One may, alternatively, represent  $f^{test}$  in terms of the entire training feature tensor as follows,

$$f^{test} = F s, \quad (12)$$

Back to our notation in Section. II,  $f^{test} = D y^{test}$  and  $F = D Y \in \mathbb{R}^{(T \times M) \times N}$  are the mappings of the test sample in addition to the constructed training tensor into the pre-designed feature space,

respectively;  $\mathbf{s} \in \mathbb{R}^N$  represents the sparse indicator vector. If (11) holds, a solution to (12) exists as  $\mathbf{s}^* = [\mathbf{0}, \dots, \mathbf{0}, \mathbf{s}_j, \mathbf{0}, \dots, \mathbf{0}]^T$ . By definition  $\mathbf{s}$  is a *sparse vector* where most of the elements are equal to zero except those associated with the  $j^{\text{th}}$  GICE class. Figure 3 illustrates a visualization of such a procedure. If  $F$  is formed from an overcomplete system of linear equations, i.e.,  $L < N$ , where  $L = T \times M$  under certain conditions, the desirable *sparse format* of  $\mathbf{s}^*$ , the solution of (12) can be found using the following optimization problem.

$$P_0: \quad \hat{\mathbf{s}}_0 = \underset{\mathbf{s}}{\operatorname{argmin}} \|\mathbf{s}\|_0 \quad \text{subject to} \quad \mathbf{f}^{\text{test}} = \mathbf{F}\mathbf{s}. \quad (13)$$

where the  $l_0$ -norm represents the number of nonzero elements in vector  $\mathbf{s}$ . In GICE classification, the training tensor  $F$  satisfies the underdetermined format, as the number of GICE classes  $J$  is reasonably large and enough number of training data points from each GICE event class  $c_j$   $\{j = 1: J\}$  exists. Since  $P_0$  is NP-hard, we can, instead, use the following relaxed  $l_1$ -norm problem:

$$P_{N1}: \quad \hat{\mathbf{s}}_1 = \underset{\mathbf{s}}{\operatorname{argmin}} \|\mathbf{s}\|_1 \quad \text{subject to} \quad \|\mathbf{f}^{\text{test}} - \mathbf{F}\mathbf{s}\|_2 < \eta. \quad (14)$$

Which is equivalent to the Basic Pursuit Denoising regularization. Variety of optimization and greedy based sparse solvers are available for solving  $P_{N1}$  and the mathematical requirements for the exact recovery of the sparse signal  $\mathbf{s}$  has been widely discussed in the literature [19], [3] (and references there in).

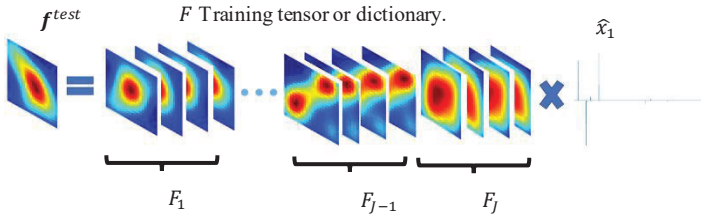


Fig. 3. A 3D Visualization of the details of the mathematical solution of TISC-GIC for a test data sample

### B. Notable Properties of TISC-GIC Approach

1. Our approach exploits the simultaneous 3-Phase information through defining an alternative complex signal (2) compared to the single-phase analysis, which results in missing potential couplings between-phase relations such as unbalance.

2. With regards to the fact of “blessing of dimensionality” [19], we can perform a random projection from feature space  $F$  to an alternative lower-dimensional feature space while not sacrificing the recovery performance. This is equivalent in TISC-GIC, to generate random faces from time-frequency images of the HSCA.

3. Informative sample selection can also be approached to further optimize the number of training samples used to form the training matrix  $F$  (12). Significantly reducing the size of this matrix and thereby, the computational cost, Algorithm.1 achieves this goal [21].

4. Regarding our discussions in Section VI-A, due to the unique formulation of sparse based classification, surprisingly, the more the number of GICE classes in TISC-GIC, the sparser the pattern of signal  $\mathbf{s}$  and the better the overall recovery performance of (14).

### Algorithm 1. Informative Data Samples Selection [3]

---

**input:** Dimensionality optimized training dictionary  $A \in \mathbb{R}^{L \times N}$

- 1- Initiate  $A$  with any arbitrary extreme point of  $A$ .
- 2- Find the best element that minimizes the Hausdorff distance.
 
$$a_j^* = \underset{a_j \in A \setminus A}{\operatorname{argmin}} d_H(A \cup a_j, A).$$
- 3-  $A \leftarrow A \cup a_j^*$ .
- 4- Return to step 1 if the desired  $\hat{N}$  or  $\epsilon$  is not achieved.

**output:** Approximated training dictionary  $A \in \mathbb{R}^{L \times \hat{N}}$

---

Let  $F = DY$  be the training tensor created using the data points of  $J$  number of GICE classes. Also, for a given  $\mathbf{f}^{\text{test}}$ , let  $\hat{\mathbf{s}}_1$  be the optimal solution of  $P_{N1}$ . The selected class is attributed to a sub-segment in vector  $\hat{\mathbf{s}}_1$  that has the minimum reconstruction residual value. Figure 3 is a visualization of a typical SRC procedure for a GICE event (Algorithm.2).

### Algorithm 2. Sparse GICE Events Classifier (TISC)

---

**input:** training data matrix  $\mathbf{Y} \in \mathbb{R}^{M \times N}$ , GIC test sample  $\mathbf{y}^{\text{test}} \in \mathbb{R}^M$

1. Extract the feature matrix from the training data, using a random transformation matrix  $\mathbf{D} \in \mathbb{R}^{L \times M}$ :  $\mathbf{F} = \mathbf{D}\mathbf{Y} \in \mathbb{R}^{L \times N}$ . Feature extraction procedure.
2. Extract features of the testing data from the test sample, using the matrix  $\mathbf{D}$  used in step 1:  $\mathbf{f}^{\text{test}} = \mathbf{D}\mathbf{y}^{\text{test}}$ .
3. Calculate the approximated training dictionary  $\mathbf{A}$  using Algorithm 1.
4. Solve  $P_1$  or  $NP_1$  for sparse vector  $\hat{\mathbf{x}}_1$ .
5. Compute  $J$  purified vectors  $\hat{\mathbf{x}}_1^j$  for  $j = 1, \dots, J$ , using indicator function  $g(\hat{\mathbf{x}}_1): \mathbb{R}^L \rightarrow \mathbb{R}^L$ , such that  $\hat{\mathbf{x}}_1^j = g(\hat{\mathbf{x}}_1)$ , is a new vector whose only nonzero entries are the entries in  $\hat{\mathbf{x}}_1$  that are associated with class  $c_j$ .
6. Compute residual  $r_j = \|\mathbf{f}^{\text{test}} - \mathbf{F}^j \hat{\mathbf{x}}_1^j\|_2$  for  $j = 1, \dots, J$ .
7.  $j^* = \underset{j=1, \dots, J}{\operatorname{argmin}} r_j$ .

**output:** Classify  $(\mathbf{y}^{\text{test}}) \triangleq c_{j^*}$

---

## V. RESULTS AND DISCUSSIONS

### A. Data and Feature Vectors Generation

The overall performance GIC-SRC framework has been verified over a synthesized 3- $\phi$  database that has been generated as directed in [22]-[23]. A set of 1000 event samples per class, has been generated for DC saturation (caused by GIC), normal operational condition, and AC saturation scenarios each one associated with three operational conditions including harmonic distortions caused by nonlinear loads, in addition to out-of-band interferences (OBI), and a normal waveform [23]. Therefore, 12 types of event waveforms are generated in total. The signal to noise ratio (SNR) of all waveforms is set within 20-50 dB, randomly, to approximate the measurement noises.

To apply the S-transform on 3- $\phi$  signals first, d-q decomposition is applied to map the current signals from the original 3-D  $i_{abc}$  domain to  $i_{dq}$  domain. The  $d, q$  components are merged and formed a complex representation for the current signal:  $i_{dq}(t) = I_d(t) + jI_q(t)$ . Fig 4.a-d are illustrating the  $I_d(t)$ , blue, and  $I_q(t)$ , red, components for a couple of selected saturation-related events.

TABLE I. GENERATED TRANSFORMER SATURATION-RELATED EVENTS SPECIFICATIONS [22]

Test Case	Saturation Type		
	AC	DC	NO
Saturation level	0.001pu-0.15pu	0.001pu-0.15pu	0
Harmonic Distortion	0.5 %-10 % THD; random choose up to 50 <sup>th</sup> order		
Out-of-Band	10Hz to 120Hz; level 0.01pu-0.1pu		
Nonlinear Load	1% to 20% of total load		

TABLE II. COMPARISON OF THE CLASSIFICATION ACCURACY (%) FOR 9 COMBINED FEATURE-CLASSIFIER APPROACHES: A 10-FOLD EVALUATION FRAMEWORK

FE/Classifier	SRC (TISC)	RBFNN	RBF SVM	Average
STFT	<b>81.4</b>	71.2	73.9	75.5
WT	77.1	69.6	<b>77.3</b>	74.6
HST	<b>83.6</b>	75.5	79.7	<b>79.6</b>
Average	<b>80.7</b>	72.1	76.6	#

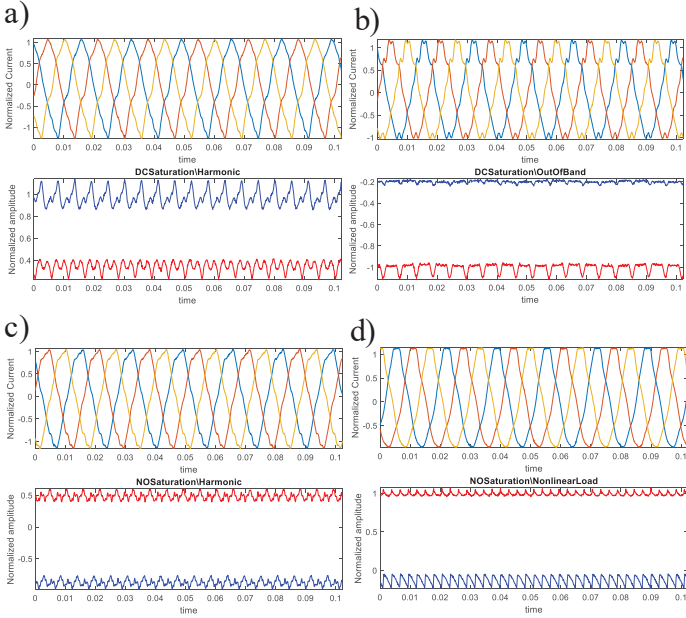


Fig 4. a-d are illustrating the  $I_d(t)$ , blue, and  $I_q(t)$ , red, components for a) DC Saturation with Harmonics, b) DC Saturation with Out of Band effect, c) Pure harmonic and d) a nonlinear load condition

## B. Results

In addition to TISC-GIC we have designed and evaluated an RBF neural network and an RBF support vector machine. Table I is summarizing the average identification accuracy rate overall 12 event classes for SRC vs. RBF-NN, and RBF-SVM using STFT, Gabor WT, and HS-Transforms scalograms (for more information regarding the details of the ANN and SVM approaches please refer to [15]-[16]). The set of 1000 originally generated data samples of each Saturation or GIC event class has been split into 10 subgroups of 100 data samples. Then a  $k$ -fold approach has been used to fairly test and verifies the performance of each of the 9 feature-classifier combinations as listed in Table II. In  $k$ -fold verification, in each fold, 100 data points have been reserved as test and the rest of the 900 data samples are used for training purposes. The average test performance over 10 folds is taken as the overall classification accuracy for each data class. Finally, the average classification for all 12 classes of events have been calculated for each combination of feature-classifier framework and reported in Table II. As it can be seen, the average performance of all approaches is higher with HS-transform FE, (above 75%), while SVM slightly leads in the WT and SRC leads with a considerable margin in both STFT and HS-Transforms.

Since by using the whole 900 training samples, the vertical size of the training matrix  $F$  in (14) would be considerably large (900 num-train-smp $\times$ 12 num-class), Algorithm 1 is applied to select the most informative data sample for each data class. The first 200

identified convexhull vertices are selected as the most informative data samples, and the same 10-fold classification verification is performed. We observed that the classification accuracy has been only varied within -0.04% for HSF-SRC and -1.8% for STFT-RBFNN. Considering the train-free functionality of the TISC-GIC to ANN, SVM and the results obtained from the DNN [22], this is a promising alternative to GIC events detection and classification well-suited for low computational resources in observational devices such as PMUs and inverters.

## VI. CONCLUSIONS

In this paper, combining the unique time-frequency properties of a modified version of Stockwell Transform named Hybrid S-Transform with the theory of sparse representation-based classification, we proposed a linear Time-frequency-based formulation for GIC event classification termed as TISC-GIC classifier. The main privileges of the proposed framework compared to the state-of-the-art techniques are Training-free property, feature selection independency, which eliminates all the required effort and time for FE-FS and training steps. On top of that, the linearity of GIC-SRC significantly decreases the time complexity while can easily handle the integration of a greater number of event classes within a simple matrix concatenation step (12). We verified our approach over a comprehensive set of 12 GIC polluted signal patterns generated using the IEEE standard models and compared the classification accuracy vs ANN and SVM machine as two highly recognized artificial intelligence-based classification paradigms.

## REFERENCES

- [1] Overbye, Thomas J., Trevor R. Hutchins, Komal Shetye, Jamie Weber, and Scott Dahman. "Integration of geomagnetic disturbance modeling into the power flow: A methodology for large-scale system studies." In *2012 North American Power Symposium (NAPS)*, pp. 1-7. IEEE, 2012.
- [2] Chen CI, Chen YC. Intelligent identification of voltage variation events based on IEEE Std 1159-2009 for SCADA of distributed energy system. *IEEE Transactions on Industrial Electronics*. 2014 Aug 19;62(4):2604-11.
- [3] Babakmehr, M., Sartipizadeh, H. and Simoes, M.G., 2019. Compressive Informative Sparse Representation-based Power Quality Events Classification. *IEEE Transactions on Industrial Informatics*.
- [4] Ray, Prakash K., Nand Kishor, and Soumya R. Mohanty. "Islanding and power quality disturbance detection in grid-connected hybrid power system using wavelet and S-S-transform." *IEEE Transactions on Smart Grid* 3, no. 3 (2012): 1082-1094.
- [5] CH, RAMI REDDY, and K. Harinadha Reddy. "Islanding Detection Techniques for Grid Integrated DG-A Review." *International Journal of Renewable Energy Research (IJRER)* 9, no. 2 (2019): 960-977.

- [6] Walling, Reigh A. "Potential impacts of harmonics on bulk system integrity during geomagnetic disturbances." In *2013 IEEE Power & Energy Society General Meeting*, pp. 1-5. IEEE, 2013.
- [7] Medeiros, Rodrigo Prado, and Flavio Bezerra Costa. "A wavelet-based transformer differential protection with differential current transformer saturation and cross-country fault detection." *IEEE Transactions on Power Delivery* 33, no. 2 (2017): 789-799.
- [8] Ripka, Pavel, Karel Draxler, and Renata Styblikova. "Measurement of DC currents in the power grid by current transformer." *IEEE transactions on magnetics* 49, no. 1 (2012): 73-76.
- [9] Stockwell, Robert Glenn, Lalu Mansinha, and R. P. Lowe. "Localization of the complex spectrum: The S transform." *IEEE transactions on signal processing* 44, no. 4 (1996): 998-1001.
- [10] Harirchi, F. and Simoes, M.G., 2018. Enhanced instantaneous power theory decomposition for power quality smart converter applications. *IEEE Transactions on Power Electronics*, 33(11), pp.9344-9359.
- [11] Hlawatsch F, Boudreaux-Bartels GF. Linear and quadratic time-frequency signal representations. *IEEE signal processing magazine*. 1992 Apr 2;9(2):21-67.
- [12] Stockwell, Robert Glenn. "A basis for efficient representation of the S-transform." *Digital Signal Processing* 17, no. 1 (2007): 371-393.
- [13] Hlawatsch, F. and Boudreaux-Bartels, G.F., 1992. Linear and quadratic time-frequency signal representations. *IEEE signal processing magazine*, 9(2), pp.21-67.
- [14] Brown, Robert A., M. Louis Lauzon, and Richard Frayne. "A general description of linear time-frequency transforms and formulation of a fast, invertible transform that samples the continuous S-transform spectrum nonredundantly." *IEEE Transactions on Signal Processing* 58, no. 1 (2009): 281-290.
- [15] Mohanty, S. R., Kishor, N., Ray, P. K., & Catalo, J. P. (2014). Comparative study of advanced signal processing techniques for islanding detection in a hybrid distributed generation system. *IEEE Transactions on sustainable Energy*, 6(1), 122-131.
- [16] Merlin, Victor Luiz, Ricardo Caneloi dos Santos, A. P. Grilo, J. C. M. Vieira, Denis Vinicius Coury, and Mário Oleskovicz. "A new artificial neural network-based method for islanding detection of distributed generators." *International Journal of Electrical Power & Energy Systems* 75 (2016): 139-151.
- [17] Biswal, Birendra, Pradipta K. Dash, and Bijaya K. Panigrahi. "Non-stationary power signal processing for pattern recognition using HS-transform." *Applied Soft Computing* 9, no. 1 (2009): 107-117.
- [18] Ashrafian, A., M. Rostami, and G. B. Gharehpetian. "Hyperbolic S-transform-based method for classification of external faults, incipient faults, inrush currents and internal faults in power transformers." *IET generation, transmission & distribution* 6.10 (2012): 940-950.
- [19] Wright, John, Allen Y. Yang, Arvind Ganesh, S. Shankar Sastry, and Yi Ma. "Robust face recognition via sparse representation." *IEEE transactions on pattern analysis and machine intelligence* 31, no. 2 (2008): 210-227.
- [20] Majidi, Mehrdad, Mohammed Sami Fadali, Mehdi Etezadi-Amoli, and Mohammad Oskuoee. "Partial discharge pattern recognition via sparse representation and ANN." *IEEE Transactions on Dielectrics and Electrical Insulation* 22, no. 2 (2015): 1061-1070.
- [21] Sartipizadeh, H., & Vincent, T. L. (2016). Computing the approximate convex hull in high dimensions. *arXiv preprint arXiv:1603.04422*.
- [22] Wang, Shiyuan, Payman Dehghanian, Li Li, and Bo Wang. "A machine learning approach to detection of geomagnetically induced currents in power grids." *IEEE Transactions on Industry Applications* (2019).
- [23] Becejac, T., Dehghanian, P. and Kezunovic, M., 2016, October. Probabilistic assessment of PMU integrity for planning of periodic maintenance and testing. In *2016 International Conference on Probabilistic Methods Applied to Power Systems (PMAPS)* (pp. 1-6). IEEE.
- [24] Harirchi, F., Hadidi, R., Babakmehr, M., & Simões, M. G. (2019, May). Advanced Three-Phase Instantaneous Power Theory Feature Extraction for Microgrid Islanding and Synchronized Measurements. In *2019 International Conference on Smart Grid Synchronized Measurements and Analytics (SGSMA)* (pp. 1-8). IEEE.